

Source Coding Based mmWave Channel Estimation with Deep Learning Based Decoding

Yahia Shabara, Eylem Ekici and C. Emre Koksal
 Department of Electrical and Computer Engineering
 The Ohio State University, Columbus, Ohio 43210
 Email: {shabara.1, ekici.2, koksal.2}@osu.edu

Abstract—mmWave technology is set to become a main feature of next generation wireless networks, e.g., 5G mobile and WiFi 802.11ad/ay. Among the basic and most fundamental challenges facing mmWave is the ability to overcome its unfavorable propagation characteristics using energy efficient solutions. This has been addressed using innovative transceiver architectures. However, these architectures have their own limitations when it comes to channel estimation. This paper focuses on *channel estimation* and poses it as a source compression problem, where channel measurements are designed to mimic an encoded (compressed) version of the channel. We show that linear source codes can significantly reduce the number of channel measurements required to discover all channel paths. We also propose a deep-learning-based approach for decoding the obtained measurements, which enables high-speed and efficient channel discovery.

I. INTRODUCTION

Wireless networks today carry billions of gigabytes of data per month. Meanwhile, the global mobile data traffic is expected to increase at a compound annual growth rate of 47% to reach 49 exabytes by the year 2021 [1]. In order to meet this ever-increasing data traffic demand, next-generation wireless networks are bound to exploit the under-utilized millimeter wave (mmWave) frequency band [2]–[4] which promises orders of magnitude increase in data rates due to the large bandwidth available compared to sub-6 GHz frequencies. mmWave, however, is hampered with severe path losses [?] which render its propagation characteristics unfavorable. To overcome this hindrance, large gain, highly-directional antenna arrays are proposed as a counter measure. The idea here is to design antennas with large enough aperture that generate narrow beam patterns which can concentrate the transmitted power into small angular directions. This way, signals can travel longer distances under strong attenuation. Fortunately, this is made possible by the small wavelength of mmWave signals which allows tens or hundreds of antenna elements to be packed in typical-sized mobile devices. The narrow beam design is also great for *spatial reuse* where multiple communication links can, simultaneously, be active with minimal interference [5].

Large antenna arrays, however, create other challenges. For example, the use of traditional, fully-digital transceivers has been ruled out due to their high power consumption. This prompted studying alternative energy-efficient transceiver architectures including *analog* and *hybrid* transceivers as well

as transceivers with a network of switches between its antennas and RF chains [6]. In general, different transceivers have varying architectural complexity and are associated with different levels of energy consumption. They also pose several challenges to channel estimation, transmit-precoding and receive-combining. Moreover, the narrow beams make maintaining TX-RX alignment very sensitive to blockage and mobility.

In this work, *we focus on the problem of channel estimation* in mmWave communication networks. The challenges of this problem arise due to the large antenna arrays employed at TX and RX combined with the limited capabilities of the commonly considered energy-efficient transceivers. In particular, the time overhead associated with estimating the mmWave channel matrix can be quite large. Hence, reducing the number of channel measurements is a critical step to facilitate mmWave networks. This is especially crucial due to the relatively short coherence time of mmWave channels¹. Fortunately, reducing the number of measurements does not necessarily decrease the quality of channel estimation. This is due to the sparse nature of mmWave channels; a feature that has been revealed by empirical measurement studies [4], [8] and further adopted by statistical mmWave channel models [?].

Numerous solutions for reducing the number of channel measurements have been proposed in literature with *Compressed Sensing* at the center of most of these solutions [9]. Compressed sensing is a technique used to recover sparse signals from a small number of linear measurements. The essence of compressed sensing is that if the measured signal is known to be compressible (by some transform coding), then we could reliably recover the signal using an under-determined system of linear measurements. Other approaches also include measurements with hierarchical beam patterns that sequentially narrow down the angular direction(s) containing channel paths, and measurements with overlapped beam patterns where each measurement combines signals received from random angular directions [10]. In this paper, however, we propose an alternative approach that is directly inspired by *source coding (data compression)*.

Solution Overview: In the source coding problem, the objective is to encode information sequences using codewords

¹The coherence time is inversely proportional to carrier frequency (and the Doppler spread) [7]

with smaller expected length. The idea here is to get rid of redundancies in the source and obtain shorter, more efficient, representation for the data. This problem is well studied and many source compression codes have been developed. Now, if we imagine that mmWave channels are information sequences, then we can use source codes to encode them and generate shorter channel representations. Then, by designing the *channel measurements* to be equivalent to encoded channels, we can significantly reduce the number of required measurements. This number is dependent on the compression ratio of the used code and the sparsity structure of the channel.

The obvious impediment to making this idea work is that source codes are originally designed to encode information sequences that take values from *finite fields*, e.g., the binary field \mathbb{F}_2 . On the other hand, channel matrices take values from the complex field \mathbb{C} . In this paper, we will extend the use of source codes to information sequences with complex values. We will also design channel measurements such that they imitate the encoding function of specific source codes. Finally, we will map the channel measurements to their corresponding estimated channels which is analogous to *decoding* the codewords in source coding. The framework described in this paper accounts for the channel size (i.e., number of antenna elements in antenna arrays) and its sparsity level.

We only focus on *linear* source codes² in this paper, which translates in linear mapping between the channel vectors and their respective measurements. The key contributions of this work can be summarized as follows:

- A direct analogy between path discovery of mmWave channels and the problem of source compression is provided. We show that linear source codes could be efficiently utilized to design channel measurements that can be uniquely mapped to the measured channels.
- The number of required channel measurements is shown to be dependent on the compression ratio of the chosen source code.
- The complex function of decoding the observed measurements is achieved using supervised deep learning, which enables very high speed processing.

Related Work: Both compressed sensing and our proposed source coding based solution share the concept of compressibility of the source. However, compressed sensing uses random linear combinations of the observed sparse source to obtain the measurements vector (e.g., with coefficients $\sim \mathcal{N}(0, 1)$). When this solution is incorporated in mm-wave channel estimation, it translates into designing antenna beam patterns of highly irregular shapes. Such beam patterns are difficult to obtain and are sensitive to the presence of side lobes, beam overlap and resolution of phase quantizers. On the other hand, the source coding based solution allows for better

²These are codes where a linear transformation between the original information sequences and their corresponding encoded ones exists. The linear transformation is given by a generator matrix, denoted by $\mathbf{G} \in \{0, 1\}^{m \times n}$. Specifically, if $\mathbf{x} \in \{0, 1\}^n$ and $\mathbf{s}_x \in \{0, 1\}^m$ are column vectors that denote the original information sequence and its code under \mathbf{G} , respectively, then, we have that $\mathbf{s}_x = \mathbf{G}\mathbf{x}$.

structure of antenna patterns. Precisely, for each measurement, a specific angular direction is either included (with constant gain/coefficient) or is excluded. This will be discussed in details in Section II and highlighted in Fig. 2.

Our earlier work in [11] presented a “Linear Block Coding” (LBC) based solution for mmWave channel estimation, where we drew an analogy between mmWave path discovery and error discovery in channel codes. Source compression, however, is a more natural fit for this problem. Further, it enables us to evaluate basic fundamental limits on the minimum number of measurements needed for certain levels of performance. The solution in [11] is in fact a special case of our source-coding-based solution since LBCs can be used as syndrome source codes [12].

Similar to [10], our proposed solution also uses the idea of designing overlapped antenna beams to obtain the channel measurements. However, the angular directions whose beams are overlapped is going to be exactly determined by some corresponding source code instead of being randomly selected like in [10]. This makes our solution capable of discovering multiple channel paths unlike [10] which still has to account for the existence of multiple paths to determine the number of measurements but can only discover the strongest one.

Decoding the obtained measurements can be achieved using a variety of tools including: i) the “look-up” table method, proposed in [13], which is only suitable for transceivers with few-bit ADCs, ii) the “search” method which entails a combinatorial search over the column space of the sensing matrix [13] and iii) the “Approximate Message Passing” (AMP) algorithms [14] and their variants, e.g., GAMP/VAMP [15], among other methods. These methods widely vary in computational complexity and accuracy. In general, the more accurate methods require higher computational complexity. Alternatively, in this paper, we propose a Deep Learning (DL) approach for decoding the measurements which promises high-speed, yet accurate decoding. Deep learning is very powerful in extracting patterns from large amounts of data. It has been widely used in problems of computer vision, speech recognition and natural language processing. Recently, it has also been applied to problems in electrical communications [16], including, but not limited to channel estimation [17], [18].

II. MOTIVATING EXAMPLE

We present a simple illustrative example that highlights the features of our proposed source coding-based beam discovery.

Problem set-up: Consider a point-to-point mm-wave channel with single transmit-multiple receive antennas. The transmitter, having just one antenna, can only perform omni-directional transmission. The receiver, on the other hand, is capable of forming directional antenna beam patterns. However, initially, the receiver does not know which direction offers the highest TX signal power. To acquire such knowledge, the receiver performs several channel measurements, the results of which will determine the optimal direction for its beam alignment.

Channel description: Let $n_t = 1$ and $n_r = 15$ denote the

number of TX and RX antennas, respectively, and let $\mathbf{q} = (q_0 \ q_1 \ \dots \ q_{14})^T$ denote the corresponding 15×1 channel vector where q_i represents the channel gain between the TX antenna and the i^{th} RX antenna. Let the corresponding angular (virtual) channel of \mathbf{q} be denoted by \mathbf{q}^a such that

$$\mathbf{q}^a = (q_0^a \ q_1^a \ \dots \ q_{14}^a)^T, \quad (1)$$

where q_i^a 's are the channel gain values received from different AoAs. Note that \mathbf{q}^a can be mapped to and from \mathbf{q} using the unitary Discrete Fourier Transform (DFT) matrix \mathbf{U}_r such that $\mathbf{q}^a = \mathbf{U}_r^H \mathbf{q}$ (this linear transformation and the construction of \mathbf{U}_r will be described in detail in Section III). Interested readers can find more details in [7, Chapter 7.3.4]).

We assume a *single-path* channel where only one path between TX and RX may exist. Let the path gain be denoted by α . For simplicity, let $\alpha = 1$. Further, let us assume a perfect sparsity model where the AoA of the channel path, if it exists, lie along one of the AoAs defined in \mathbf{U}_r . Thus the path gain only contributes to a single component in \mathbf{q}^a . This means that, if a channel path exists, then $\exists i_0$ such that $q_{i_0}^a = 1$ while $q_i^a = 0 \ \forall i \neq i_0$, otherwise $q_i^a = 0 \ \forall i$.

Channel measurements: The TX sends pilot symbols of the form $x=1$, while the RX observes a vector of size 15×1 , denoted by \mathbf{y} , at its antenna array. This can be represented as

$$\mathbf{y} = \mathbf{q}x = \mathbf{q}. \quad (2)$$

Thus, the received vector \mathbf{y} is exactly the channel vector we want to estimate. We also have that $\mathbf{y}^a = \mathbf{U}_r^H \mathbf{y} = \mathbf{q}^a$ is the received vector represented in the angular domain. The receiver performs a sequence of channel measurements using different *receive combining* (rx-combining) vectors \mathbf{w}_i . We denote the i^{th} measurement symbol by y_i^s such that

$$y_i^s = \mathbf{w}_i^H \mathbf{y} = \mathbf{w}_i^H \mathbf{q}. \quad (3)$$

The collection of all measurements forms the measurement vector \mathbf{y}^s where

$$\mathbf{y}^s = (y_0^s \ y_1^s \ \dots \ y_{m-1}^s)^T. \quad (4)$$

Objective: Find the best direction of beam alignment at RX using fewest number of measurements.

Solution: We will describe two solutions for this problem; one that is simple but requires a large number of measurements and another more clever one that requires fewer measurements.

(i) **Simple solution:** This is the straightforward approach of scanning the channel, one AoA direction at a time. That is, we sequentially focus the antenna beam pattern at one specific AoA direction to obtain its corresponding channel gain component. Fig. 1 depicts all 15 possible antenna beam patterns, each of which can be obtained using a specific design of \mathbf{w}_i . Accordingly, the number of required measurements is $m = n_r = 15$.

(ii) **Source-Coding-Based solution:** Based on the channel description provided above, we can think of \mathbf{q}^a as an information sequence of length 15 produced by a *binary* information source (since $q_i^a \in \{0, 1\}$). If we behold this information

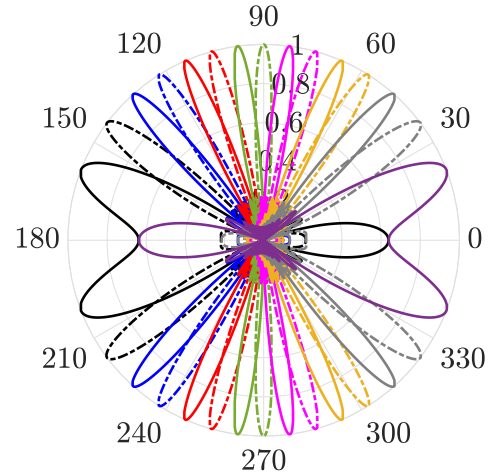


Fig. 1: All the possible 15 antenna beams.

theoretic view of the channel vector, then we can see that \mathbf{q}^a contains a lot of redundant information. This redundancy can be reduced using source coding techniques which can produce shorter *codewords* that represent the channels. Then, we can design channel measurements \mathbf{y}^s such that each measurement produces a single component of its corresponding codeword (compressed channel vector). The main result of this paper is that, by carefully choosing a source code, a one-to-one mapping between the measurements, \mathbf{y}^s , and \mathbf{q}^a exists.

We model the channel as a *binary data source* that emits one of 16 possible channel vectors; 15 of which represent the case of a single path existing at one of the 15 components of \mathbf{q}^a plus the $\mathbf{0}$ vector which represents the case of no existing paths in the channel. Let \mathcal{Q}^a denote the set of all possible angular channel vectors. Hence, $|\mathcal{Q}^a| = 16$. We will shortly explain the details of encoding \mathbf{q}^a and how measurements that mimic the encoding function are designed, but let us first discuss the lower bound on the number of measurements using this approach. Let $\mathbb{P}(\mathbf{q}^a)$ denote the probability of occurrence of $\mathbf{q}^a \in \mathcal{Q}^a$. Suppose that all 16 channel vectors in \mathcal{Q}^a have equal probability of occurrence. Thus, $\mathbb{P}(\mathbf{q}^a) = \frac{1}{16} \ \forall \mathbf{q}^a \in \mathcal{Q}^a$. Then, we can find the *entropy*, denoted by H_2 , of the aforementioned data source as:

$$H_2(\mathbf{q}^a) = \sum_{\mathbf{q}^a \in \mathcal{Q}^a} \mathbb{P}(\mathbf{q}^a) \log_2 \left(\frac{1}{\mathbb{P}(\mathbf{q}^a)} \right) = 4 \quad (5)$$

Therefore, assuming equiprobable channel outcomes, the minimum number of bits that can be used to represent the channel vector *using our binary source coding technique* is 4. It is important to note here that the entropy is *not* a general lower bound on the number of measurements but only a lower bound for techniques that adopt binary source coding algorithms in mm-wave channel estimation problems. For this particular example, we can find a source code that achieves this bound which we are going to present next.

Let us design the measurements vector, \mathbf{y}^s , such that

$$\mathbf{y}^s \equiv \mathbf{G} \mathbf{q}^a, \quad \text{where} \quad (6)$$

TABLE I: Channel measurements \mathbf{y}^s corresponding to all $\mathbf{q}^a \in \mathcal{Q}^a$

Channel measurement \mathbf{y}^{sT}	Angular Channel \mathbf{q}^{aT}
0000	0000000000000000
1000	1000000000000000
0100	0100000000000000
0010	0010000000000000
0001	0001000000000000
1100	0000100000000000
0110	0000010000000000
0011	0000001000000000
1101	0000000100000000
1010	0000000010000000
0101	0000000001000000
1110	0000000000100000
0111	0000000000010000
1111	0000000000000100
1011	0000000000000010
1001	0000000000000001

$$\mathbf{G} = \begin{pmatrix} 1 & 0 & 0 & 0 & 1 & 0 & 0 & 1 & 1 & 0 & 1 & 0 & 1 & 1 & 1 \\ 0 & 1 & 0 & 0 & 1 & 1 & 0 & 1 & 0 & 1 & 1 & 1 & 1 & 0 & 0 \\ 0 & 0 & 1 & 0 & 0 & 1 & 1 & 0 & 1 & 0 & 1 & 1 & 1 & 1 & 0 \\ 0 & 0 & 0 & 1 & 0 & 0 & 1 & 1 & 0 & 1 & 0 & 1 & 1 & 1 & 1 \end{pmatrix} \quad (7)$$

is the generator matrix of a linear source code C (recall footnote 2). More specifically, C is the (15, 11, 3) Hamming code used as a *syndrome source code* [12]. Now, we have that each y_i^s is obtained by multiplying the i^{th} row of \mathbf{G} by $\mathbf{q}^a \xrightarrow{\text{i.e.}}$ $y_i^s = \sum_j g_{i,j} \times q_j^a$. Hence the i^{th} channel measurement linearly combines all angular channel gain components q_j^a for all j such that $g_{i,j} = 1$. Such linear combination is achieved using a carefully designed \mathbf{w}_i (recall Eq.(3)). Essentially, this means that in each of the measurements y_i^s , we combine the signals received at a specific set of AoA directions. These combinations are dictated by the code C **which is chosen to guarantee that each and every $\mathbf{q}^a \in \mathcal{Q}^a$ can be uniquely mapped to a corresponding measurement vector \mathbf{y}^s** . Take for example the 4th and final measurement. Since the 4th row of \mathbf{G} is given by [0 0 0 1 0 0 1 1 0 1 0 1 1 1 1], then in y_4^s we combine the signals coming from the directions {4, 7, 8, 10, 12, 13, 14, 15}. This process is depicted in Fig. 2. Table I shows all channel vectors in \mathcal{Q}^a and their corresponding measurement vectors.

In the following sections, we will formally introduce the concepts and ideas demonstrated in this motivating example. We will embrace the practical considerations of multi-path channels and arbitrary path gain values (i.e., $\alpha \in \mathbb{C}$). We will also take into account the channel noise and finite quantization.

III. SYSTEM MODEL

We consider point-to-point mm-wave channels with n_t and n_r antennas at TX and RX, respectively. Antennas at both TX and RX sides form Uniform Linear Arrays (ULA) where every antenna element is connected to a phase-shifter and a low-power variable-gain amplifier. On the TX side, a single RF chain feeds its ULA through an n_t -way power splitter, while on the RX side, the outputs of the ULA, after being processed by amplifiers and phase-shifters, are then linearly combined using an adder and fed through to a single RF chain with in-phase (I) and quadrature (Q) channels. Two mid-tread ADCs

with 2^b+1 levels are used to quantize the I and Q components of the received signal. Here, the term b loosely denotes to the number of bits that describes the resolution of the used ADCs. Fig. 3 depicts the transceiver architecture we just described.

We assume single-tap channels where all channel paths have just one significant tap. We also adopt a channel clustering model where paths between TX and RX form clusters in the angular domain [2], [8]. Let L denote the number of available channel clusters. Due to the sparse nature of mm-wave channels, only a limited number of clusters exist³, where $L \ll n_r, n_t$. We assume that each cluster contains only one path since distinct paths within each cluster cannot typically be resolved. Each channel path (e.g., l^{th} path) is attributed with an AoD θ_l , an AoA ϕ_l and a path gain α_l . Let $\alpha_l^b \in \mathbb{C}$ denote the baseband path gain such that

$$\alpha_l^b = \alpha_l \sqrt{n_r n_t} e^{-j \frac{2\pi \rho_l}{\lambda_c}}, \quad (8)$$

where ρ_l is the path length and λ_c is the carrier wavelength. We define the *directional cosines* of the AoD and AoA of the l^{th} path as $\Omega_{tl} \triangleq \cos(\theta_l)$ and $\Omega_{rl} \triangleq \cos(\phi_l)$, respectively. The transmit and receive spatial signatures at an arbitrary directional cosine Ω is denoted by $\mathbf{e}_t(\Omega)$ and $\mathbf{e}_r(\Omega)$, receptively. We define $\mathbf{e}_t(\Omega)$ (and similarly $\mathbf{e}_r(\Omega)$) as:

$$\mathbf{e}_t(\Omega) = \frac{1}{\sqrt{n_t}} \left(1, e^{-j2\pi\Delta_t\Omega}, e^{-j2\pi2\Delta_t\Omega}, \dots, e^{-j2\pi(n_t-1)\Delta_t\Omega} \right)^T \quad (9)$$

where Δ_t and Δ_r are the antenna separations at TX and RX ULAs normalized by the wavelength λ_c .

Let $\mathbf{Q} \in \mathbb{C}^{n_r \times n_t}$ denote the channel matrix. Thus, we have

$$\mathbf{Q} = \sum_{l=1}^L \alpha_l^b \mathbf{e}_r(\Omega_{rl}) \mathbf{e}_t^H(\Omega_{tl}) \quad (10)$$

The corresponding angular channel of \mathbf{Q} , whose rows and columns divide the channel into resolvable RX and TX angular bins, respectively, is denoted by \mathbf{Q}^a and can be obtained as:

$$\mathbf{Q}^a = \mathbf{U}_r^H \mathbf{Q} \mathbf{U}_t. \quad (11)$$

The matrices \mathbf{U}_t and \mathbf{U}_r are the transmit and receive unitary Discrete Fourier Transform (DFT) matrices whose columns form an orthonormal basis for the transmit and receive signal spaces \mathbb{C}^{n_t} and \mathbb{C}^{n_r} , respectively. The definition of \mathbf{U}_t (likewise for \mathbf{U}_r) is given by

$$\mathbf{U}_t \triangleq \left(\mathbf{e}_t(0) \quad \mathbf{e}_t\left(\frac{1}{L_t}\right) \quad \dots \quad \mathbf{e}_t\left(\frac{n_t-1}{L_t}\right) \right), \quad (12)$$

where $L_t = n_t \Delta_t$ and $L_r = n_r \Delta_r$ denote the lengths of the TX and RX antenna arrays normalized by λ_c .

Similar to [19], [20] and [21], we assume a perfect sparsity model in which paths lie along AoD and AoA directions defined in \mathbf{U}_t and \mathbf{U}_r . Hence, each channel path only contributes to a single component of \mathbf{Q}^a . Thus, only L non-zero components in \mathbf{Q}^a exists.

³For instance, measurements carried out in New York City revealed that an average number of 2 or 3 clusters exists in mm-wave channels at 28 and 73 GHz [4].

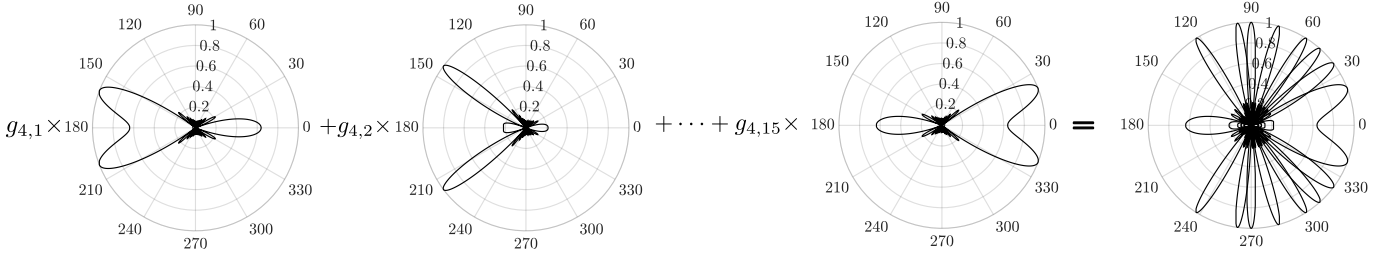


Fig. 2: Generating the beam pattern required for the 4th measurement (y_4^s)

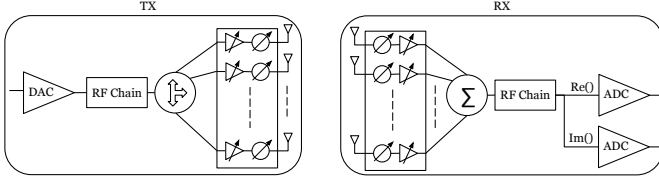


Fig. 3: Transceiver architecture: At TX, an n_t -way power splitter divides the transmit signal which is then passed through variable-gain power amplifiers and phase-shifters. A single DAC is required since the TX sends real valued signals. At RX, the acquired signal is passed through a similar network of power amplifiers and phase-shifters before being combined and fed to a single RF chain. Two ADCs are required to obtain the I/Q components of the received signal.

The transmitter sends pilot symbols s which are processed using the precoder vectors $\mathbf{f} \in \mathbb{C}^{n_t}$ to obtain the transmit vectors $\mathbf{x} = \mathbf{f}s$. The baseband channel model is given by

$$\mathbf{u}_b = \mathbf{Q}\mathbf{x} + \mathbf{n} \quad (13)$$

where \mathbf{u}_b is the received vector at the RX front end while $\mathbf{n} \sim \mathcal{CN}(\mathbf{0}, N_0 \mathbf{I}_{n_r})$ is an i.i.d. complex Gaussian noise vector. The rx-combining vectors $\mathbf{w} \in \mathbb{C}^{n_r}$ are used to obtain the received symbols $u_{i,j}$ such that

$$u_{i,j} = \mathbf{w}_i^H \mathbf{Q} \mathbf{f}_j s + \mathbf{w}_i^H \mathbf{n} \quad (14)$$

Finally, a quantized version $u_{i,j}^s$ of $u_{i,j}$ is obtained such that

$$u_{i,j}^s = [\mathbf{w}_i^H \mathbf{Q} \mathbf{f}_j s + \mathbf{w}_i^H \mathbf{n}]_+ \quad (15)$$

where $[\cdot]_+$ represents the quantization function. The noise component, normalized by $\|\mathbf{w}_i\|$ has a complex Gaussian distribution, i.e., $\frac{\mathbf{w}_i^H \mathbf{n}}{\|\mathbf{w}_i\|} \sim \mathcal{CN}(0, N_0)$. Let $y_{i,j}^s = \mathbf{w}_i^H \mathbf{Q} \mathbf{f}_j s$ denote the error-free measured symbols and let $z_{i,j} = u_{i,j}^s - y_{i,j}^s$ denote the *measurement error* which includes both channel noise and quantization error. Finally, we define the transmit SNR as

$$\text{SNR} = \frac{P}{N_0} \quad (16)$$

IV. SOURCE-CODING-BASED MEASUREMENTS

In this section, we formally introduce *mm-wave beam discovery* as a source coding problem. We initially focus on channels with single-transmit, multiple-receive antennas. We will show how to “*encode*” the channel vector into a measurement vector of fewer components. We will also show that a one-to-one mapping between the measurements

and channels exists. Then, in Section V, we will use *deep learning* techniques to decode the measurements and obtain an estimate for the observed channel. Afterwards, in Section VI, a generalized setting for channels with multiple TX and RX antennas is presented. Now, let us start our discussion with introducing some basic definitions.

Definition IV.1 (Support vector). The support vector \mathbf{v}_s associated with an arbitrary n -dimensional vector $\mathbf{v} \in \mathbb{C}^n$ is a binary vector of the same size that identifies the non-zero components of \mathbf{v} and whose components, v_{si} , are defined as

$$v_{si} = \begin{cases} 1 & , v_i \neq 0 \\ 0 & , v_i = 0 \end{cases} \quad (17)$$

Definition IV.2 (Set of Non-Zero Indexes \mathcal{X}_v). For any arbitrary n -dimensional vector \mathbf{v} , we define \mathcal{X}_v as the set of indexes of its non-zero components, i.e.,

$$\mathcal{X}_v = \{i | v_i \neq 0, 0 \leq i \leq n-1\} \quad (18)$$

Hence, if \mathbf{v}_s is the support vector corresponding to \mathbf{v} , then we have that $\mathcal{X}_v = \mathcal{X}_{\mathbf{v}_s}$, since $v_i = 0 \iff v_{si} = 0$.

A. Source Codes

Let C be a binary linear source code with encoding and decoding functions denoted by $\mathcal{E}_{\mathbb{F}_2}$ and $\mathcal{D}_{\mathbb{F}_2}$, respectively. We can just refer to C as the encoding-decoding function pair $(\mathcal{E}_{\mathbb{F}_2}, \mathcal{D}_{\mathbb{F}_2})$. The subscript \mathbb{F}_2 denotes the finite field of two elements ($0_{\mathbb{F}_2}$ and $1_{\mathbb{F}_2}$) over which the code C is defined. Later on, we will drop the subscripts to simplify notation as long as they can be inferred from the context.

Definition IV.3 (Linear Source Code). A source code C whose encoding function $\mathcal{E}_{\mathbb{F}_2}$ is a linear function of the source sequences is called a *linear source code*.

Let \mathbf{s} be a source sequence of length n where $\mathbf{s} \in \mathcal{S} \subseteq \{0_{\mathbb{F}_2}, 1_{\mathbb{F}_2}\}^n$, and let $\mathbf{c}_s \in \mathcal{I}_S \subseteq \{0_{\mathbb{F}_2}, 1_{\mathbb{F}_2}\}^m$ be its associated binary representation under C where \mathcal{I}_S is the image of \mathcal{S} under $\mathcal{E}_{\mathbb{F}_2}$. Thus, using a linear source code C , we can find the representation of \mathbf{s} under C using the following equation:

$$\mathbf{c}_s = \mathbf{G}\mathbf{s}, \quad (19)$$

where $\mathbf{G} \in \{0_{\mathbb{F}_2}, 1_{\mathbb{F}_2}\}^{m \times n}$ is called the *generator matrix*.

The decoding function $\mathcal{D}_{\mathbb{F}_2}$, maps sequences \mathbf{c}_s to a corresponding source sequence $\hat{\mathbf{s}} \in \hat{\mathcal{S}} \subseteq \{0_{\mathbb{F}_2}, 1_{\mathbb{F}_2}\}^n$.

Suppose that \mathcal{S} is the set of all sequences such that if $s_1, s_2 \in \mathcal{S}$, we have that $s_1 \neq s_2 \iff c_{s_1} \neq c_{s_2}$. In other words, $\mathcal{E}_{\mathbb{F}_2} : \mathcal{S} \rightarrow \mathcal{I}_{\mathcal{S}}$ is injective (one-to-one). Consequently, if we define the function $\mathcal{D}_{\mathbb{F}_2}$ over $\mathcal{I}_{\mathcal{S}}$ as the inverse function of $\mathcal{E}_{\mathbb{F}_2}$, i.e., $\mathcal{E}_{\mathbb{F}_2}^{-1} \triangleq \mathcal{D}_{\mathbb{F}_2} : \mathcal{I}_{\mathcal{S}} \rightarrow \mathcal{S}$, then we have that $\hat{s} = \mathcal{D}_{\mathbb{F}_2}(\mathcal{E}_{\mathbb{F}_2}(s)) = s, \forall s \in \mathcal{S}$.

B. Mm-Wave Beam Discovery

Let $\mathbf{q}^a \in \mathbb{C}^{n_r}$ denote the angular channel **vector** between TX and RX and let $\mathbf{q}_s^a \in \{0, 1\}^{n_r}$ be the support vector associated with \mathbf{q}^a such that

$$\mathbf{q}_s^a = \begin{pmatrix} q_{s_0}^a \\ q_{s_2}^a \\ \vdots \\ q_{s_{n_r-1}}^a \end{pmatrix}, \quad \text{where } q_{s_i}^a = \begin{cases} 1 & , \text{ if } q_i^a \neq 0 \\ 0 & , \text{ if } q_i^a = 0 \end{cases} \quad (20)$$

Let \mathcal{Q}^a be the set containing all possible channel vectors \mathbf{q}^a and let \mathcal{Q}_s^a be the set of all sequences \mathbf{q}_s^a such that their corresponding channel vectors $\mathbf{q}^a \in \mathcal{Q}^a$.

Remark. [Inclusion Property of \mathcal{Q}_s^a]

- (i) Let $\mathbf{q}_{s_1}^a, \mathbf{q}_{s_2}^a \in \{0, 1\}^{n_r}$ such that $\mathcal{X}_{\mathbf{q}_{s_2}^a} \subseteq \mathcal{X}_{\mathbf{q}_{s_1}^a}$. Then, we have that⁴ $\mathbf{q}_{s_1}^a \in \mathcal{Q}_s^a \implies \mathbf{q}_{s_2}^a \in \mathcal{Q}_s^a$.
- (ii) $\mathbf{0} \in \mathcal{Q}_s^a$. In fact, this is a consequence of property (i) above since for any $\mathbf{q}_s^a \in \mathcal{Q}_s^a$, we have that $\mathcal{X}_{\mathbf{0}} = \emptyset \subseteq \mathcal{X}_{\mathbf{q}_s^a}$.

Before we state the main result of this paper, let us first introduce two lemmas that are necessary for mathematical derivation.

Lemma 1. Let $\mathbf{A}_{\mathbb{F}}$ and \mathbf{A} be $n \times n$ matrices defined over \mathbb{F}_2 and \mathbb{R} , respectively. Let $a_{\mathbb{F}i,j}$, the elements of $\mathbf{A}_{\mathbb{F}}$, be scalars taken from $\{0_{\mathbb{F}_2}, 1_{\mathbb{F}_2}\}$, while $a_{i,j}$ the elements of \mathbf{A} , be scalars from $\{0, 1\} \subseteq \mathbb{R}$. Suppose that $\mathbf{A}_{\mathbb{F}}$ has non-zero determinant, i.e., $\det(\mathbf{A}_{\mathbb{F}}) \neq 0_{\mathbb{F}_2}$. If we define \mathbf{A} such that

$$a_{i,j} = \begin{cases} 0 & \text{if } a_{\mathbb{F}i,j} = 0_{\mathbb{F}_2} \\ 1 & \text{if } a_{\mathbb{F}i,j} = 1_{\mathbb{F}_2} \end{cases} \quad \forall 1 \leq i, j \leq n, \quad (21)$$

then, $\det(\mathbf{A}) \neq 0$.

Proof. Recall that the determinant of a square matrix defined over a commutative ring is given by the Leibniz formula [22]. Since \mathbb{F}_2 is a finite field (with 2 elements) then it constitutes a commutative ring. Also, we have that \mathbb{R} is a commutative ring [22]. Therefore, both determinants of $\mathbf{A}_{\mathbb{F}}$ and \mathbf{A} can be computed using the same exact formula. Since, finite field arithmetic over the prime field \mathbb{Z}_2 is the integers *modulo* 2, then we can write

$$\det(\mathbf{A}_{\mathbb{F}}) = \det(\mathbf{A}) \pmod{2} \quad (22)$$

Thus, $\exists q \in \mathbb{Z}$ (the set of integers), such that

$$\det(\mathbf{A}) = q \times 2 + \det(\mathbf{A}_{\mathbb{F}}) \quad (23)$$

$$= q \times 2 + 1 \quad (24)$$

⁴In other words, if $\mathbf{q}_{s_1}^a \in \mathcal{Q}_s^a$, then all support vectors $\mathbf{q}_{s_2}^a$ such that the non-zero components of $\mathbf{q}_{s_2}^a$ are a subset of the non-zero components of $\mathbf{q}_{s_1}^a$ also belong to \mathcal{Q}_s^a .

were the last equation follows from the fact that $\det(\mathbf{A}_{\mathbb{F}}) \neq 0_{\mathbb{F}_2} \iff \det(\mathbf{A}_{\mathbb{F}}) = 1_{\mathbb{F}_2}$. Therefore, $\det(\mathbf{A})$ is an odd integer, which implied that $\det(\mathbf{A}) \neq 0$, which concludes our proof. \square

Lemma 2. Any set of n -dimensional linearly independent vectors over \mathbb{F}_2 are also linearly independent over \mathbb{C} if we interpret their $0_{\mathbb{F}_2}$ and $1_{\mathbb{F}_2}$ components to be real scalars.

Proof. Consider a set of n -dimensional linearly independent vectors, $\mathbf{v}_1, \dots, \mathbf{v}_m$ defined over \mathbb{F}_2 . Then, construct a matrix $\mathbf{M}_{\mathbb{F}_2}$ whose columns are $\mathbf{v}_1, \dots, \mathbf{v}_m$. Since \mathbf{v}_i 's are independent, then $\mathbf{M}_{\mathbb{F}_2}$ has full column rank, i.e., $\mathbf{M}_{\mathbb{F}_2}$ is left-invertible over \mathbb{F}_2 (also m is $\leq n$). Thus $\mathbf{M}_{\mathbb{F}_2}$ has an $m \times m$ minor, call it $\mathbf{A}_{\mathbb{F}_2}$ whose determinant is non-zero. Now consider the matrix \mathbf{M} , defined over \mathbb{C} , whose elements are the 0 and 1 real scalars corresponding to the $0_{\mathbb{F}_2}$ and $1_{\mathbb{F}_2}$ values of $\mathbf{M}_{\mathbb{F}_2}$. Let \mathbf{A} be its minor corresponding to $\mathbf{A}_{\mathbb{F}_2}$ of $\mathbf{M}_{\mathbb{F}_2}$. By Lemma 1, we have that $\det(\mathbf{A}) \neq 0$. Thus, \mathbf{M} is also left-invertible which means that its columns are linearly independent. \square

Theorem 3. Consider a binary linear source code \mathcal{C} whose encoding function \mathcal{E} (defined by the binary generator matrix \mathbf{G}) is an injective function defined over $\mathcal{Q}_s^a \in \{0, 1\}^{n_r}$. Now, if we consider \mathbf{G} to be defined over the complex field, then for all channel vectors $\mathbf{q}_1^a, \mathbf{q}_2^a \in \mathcal{Q}^a \subseteq \mathbb{C}^{n_r}$ we have that $\mathbf{q}_1^a \neq \mathbf{q}_2^a$ if and only if $\mathbf{y}_1^s = \mathbf{G}\mathbf{q}_1^a \neq \mathbf{G}\mathbf{q}_2^a = \mathbf{y}_2^s$.

Proof. Let $\mathbf{q}_1^a, \mathbf{q}_2^a \in \mathcal{Q}^a$, and let $\mathbf{y}_i^s = \mathbf{G}\mathbf{q}_i^a$. Now, assume that $\mathbf{q}_1^a \neq \mathbf{q}_2^a$. Then, we have that

$$\begin{aligned} \mathbf{y}_1^s - \mathbf{y}_2^s &= \mathbf{G}\mathbf{q}_1^a - \mathbf{G}\mathbf{q}_2^a = \mathbf{G}(\underbrace{\mathbf{q}_1^a - \mathbf{q}_2^a}_{=\mathbf{v}}) = \mathbf{G}\mathbf{v} \quad (25) \\ &= \sum_{i=0}^{n_r-1} v_i \times \mathbf{g}_i = \sum_{i \in \mathcal{X}_v} v_i \times \mathbf{g}_i \quad (26) \end{aligned}$$

where $\mathbf{g}_i \forall 0 \leq i \leq n_r-1$ are the columns of \mathbf{G} .

Thus, to show that $\mathbf{y}_1^s - \mathbf{y}_2^s \neq \mathbf{0}$, we need to show that all vectors $\mathbf{g}_i \forall i \in \mathcal{X}_v$, are linearly independent. Otherwise, if such vectors \mathbf{g}_i are linearly **dependent**, then $\exists v_i \in \mathbb{R}$ for $i \in \mathcal{X}_v$ such that $\mathbf{y}_1^s - \mathbf{y}_2^s = \mathbf{G}\mathbf{v} = \mathbf{0}$.

In fact, we can show a stronger statement which is: "all vectors $\mathbf{g}_i \forall i \in \mathcal{X}_{\mathbf{q}_1^a} \cup \mathcal{X}_{\mathbf{q}_2^a} \supseteq \mathcal{X}_v$, are linearly independent". Note that $\mathcal{X}_{\mathbf{q}_1^a}$ and $\mathcal{X}_{\mathbf{q}_2^a}$ are the sets of indexes of the non-zero components of \mathbf{q}_1^a and \mathbf{q}_2^a , respectively (recall Definition IV.2) and that $\mathcal{X}_{\mathbf{q}_1^a} = \mathcal{X}_{\mathbf{q}_{s_1}^a}$ and $\mathcal{X}_{\mathbf{q}_2^a} = \mathcal{X}_{\mathbf{q}_{s_2}^a}$.

- First, let us show that \mathcal{X}_v is a subset of $\mathcal{X}_{\mathbf{q}_1^a} \cup \mathcal{X}_{\mathbf{q}_2^a}$. Since $v_i = q_{1,i}^a - q_{2,i}^a \forall 0 \leq i \leq n_r-1$, then $q_{1,i}^a = q_{2,i}^a = 0 \implies v_i = 0$. Therefore, we have that

$$\mathcal{X}_{\mathbf{q}_1^a}^c \cap \mathcal{X}_{\mathbf{q}_2^a}^c = \{\mathcal{X}_{\mathbf{q}_1^a} \cup \mathcal{X}_{\mathbf{q}_2^a}\}^c \subseteq \mathcal{X}_v^c \quad (27)$$

Then, by taking the complements of both sides we obtain the required result.

- Second, we show that the set of vectors $\mathcal{G} = \{\mathbf{g}_i | i \in \mathcal{X}_{\mathbf{q}_1^a} \cup \mathcal{X}_{\mathbf{q}_2^a}\}$ is linearly independent over $GF(2)$ (also referred to as \mathbb{F}_2).

Assume towards contradiction that \mathcal{G} is linearly dependent over $GF(2)$. Hence, there exists a set $\mathcal{G}_D \subseteq \mathcal{G}$ such that any $\mathbf{g}_{i_0} \in \mathcal{G}_D$ can be written as a linear combination of all other vectors in \mathcal{G}_D , i.e.,

$$\mathbf{g}_{i_0} = \sum_{\substack{j:j \neq i_0 \\ \mathbf{g}_j \in \mathcal{G}_D}} \mathbf{g}_j \pmod{2} \quad (28)$$

note that over $GF(2)$, we can assume, without loss of generality (W.L.O.G.), that the coefficients of the linear combination above are 1's. Hence, we have that

$$\sum_{j:\mathbf{g}_j \in \mathcal{G}_D} \mathbf{g}_j \pmod{2} = 0 \quad (29)$$

Next, assume that $\exists \mathbf{q}_{s_3}^a, \mathbf{q}_{s_4}^a \in \mathcal{Q}_s^a$ such that $\mathcal{X}_{\mathbf{v}_s} = \{j | \mathbf{g}_j \in \mathcal{G}_D\}$ where $\mathbf{v}_s = \mathbf{q}_{s_3}^a - \mathbf{q}_{s_4}^a \pmod{2}$.

Then, since \mathbf{G} is injective over \mathcal{Q}_s^a , then we have that

$$\mathbf{G}\mathbf{v}_s \pmod{2} = \sum_{j \in \mathcal{X}_{\mathbf{v}_s}} \mathbf{g}_j \pmod{2} = \sum_{j:\mathbf{g}_j \in \mathcal{G}_D} \mathbf{g}_j \pmod{2} \quad (30)$$

$$\neq \mathbf{0} \xleftrightarrow{\text{iff}} \mathbf{v}_s \pmod{2} \neq \mathbf{0} \quad (31)$$

But, if \mathcal{G}_D is non-empty, then $\mathbf{v}_s \neq \mathbf{0}$. Hence, we arrive at a contradiction to Eq. (28). Therefore, the set \mathcal{G} is linearly independent over $GF(2)$.

It remains, however, to show that such $\mathbf{q}_{s_3}^a$ and $\mathbf{q}_{s_4}^a$ indeed exist. Let us construct $\mathbf{q}_{s_3}^a$ as follows:

First, put $\mathbf{q}_{s_3}^a = \mathbf{q}_{s_1}^a$, then, reset its i^{th} component to 0 ($q_{s_3,i}^a = 0$) if $\mathbf{g}_i \notin \mathcal{G}_D$.

Similarly, set $\mathbf{q}_{s_4}^a = \mathbf{q}_{s_2}^a$, then, reset the i^{th} component to 0 ($q_{s_4,i}^a = 0$) if $\mathbf{g}_i \notin \mathcal{G}_D$ OR if $q_{s_1,i}^a = 1$.

Then, by construction, we have that $\mathcal{X}_{\mathbf{q}_{s_3}^a} \subseteq \mathcal{X}_{\mathbf{q}_{s_1}^a}$ and $\mathcal{X}_{\mathbf{q}_{s_4}^a} \subseteq \mathcal{X}_{\mathbf{q}_{s_2}^a}$. Hence, by the inclusion property (recall remark IV-B) we have that $\mathbf{q}_{s_3}^a, \mathbf{q}_{s_4}^a \in \mathcal{Q}_s^a$ since both $\mathbf{q}_{s_1}^a, \mathbf{q}_{s_2}^a \in \mathcal{Q}_s^a$. Also, it is easy to see that $q_{s_3,j}^a - q_{s_4,j}^a \pmod{2} = 1 \forall 0 \leq j \leq n_r - 1$ such that $\mathbf{g}_j \in \mathcal{G}_D$.

- Third, by Lemma 2, we have that the set \mathcal{G} , now taken over \mathbb{R} , is linearly independent.

Therefore, in Eq. (26), it follows that $\mathbf{y}_1^s - \mathbf{y}_2^s \neq \mathbf{0}$ if and only if $\mathbf{q}_1^a - \mathbf{q}_2^a \neq \mathbf{0}$ which concludes the proof. \square

C. On the lower bound on the number of measurements

In Theorem 3, we showed that a linear source code C that can **uniquely** encode all $\mathbf{q}_s^a \in \mathcal{Q}_s^a$ can be used to design a framework that uniquely measures all $\mathbf{q}^a \in \mathcal{Q}^a$. Let the compression ratio of the code C be denoted by r_c such that

$$r_c = \frac{m}{n_r} \quad (32)$$

where m and n_r are the number of rows and columns of C 's generator matrix \mathbf{G} .

Reducing the number of measurements is a fundamental objective for the mm-wave beam discovery problem. In light of Theorem 3, we can see that finding a source code with a high compression rate (small value of r_c) is crucial for attaining

such an objective. In the following discussion, we try to better understand the nature of this lower bound in the context of our proposed solution.

Corollary 3.1 . Let \underline{m} denote the lowest possible number of measurements for the linear, non-adaptive, mm-wave beam discovery problem. Then, we have that

$$\underline{m} \leq H_2(\mathbf{q}_s^a) \quad (33)$$

where $H_2(\cdot)$ is the binary entropy function.

Proof. Suppose that C is a linear source code which can uniquely compress all $\mathbf{q}_s^a \in \mathcal{Q}_s^a$. By Theorem 3, we have that the number of measurements needed for estimating the mm-wave channel can be made equal to, m ; the length of encoded channel support vectors (sequences). Since the length of compressed sequences for any such code is lower bounded by $H_2(\mathbf{q}_s^a)$ (recall Eq. 5) and since there exist optimal codes that can achieve this lower bound (see Section ?? for an example), then $\underline{m} \not\prec H_2(\mathbf{q}_s^a) \implies \underline{m} \leq H_2(\mathbf{q}_s^a)$ \square

V. MEASUREMENTS DECODING

Designing channel measurements that have one-to-one correspondence with \mathbf{q}^a is only part of the solution. Equally important, however, is the ability to map \mathbf{y}^s back to \mathbf{q}^a . In our source coding framework, this is analogous to **decoding**. The one-to-one correspondence between \mathbf{q}^a and \mathbf{y}^s guarantees that there exists an inverse function that maps \mathbf{y}^s back to \mathbf{q}^a . Nevertheless, since we can only obtain \mathbf{u}^s ; an error-corrupted version of \mathbf{y}^s , we cannot exactly regenerate \mathbf{q}^a back from \mathbf{u}^s , but rather, an estimate $\hat{\mathbf{q}}^a$. Given that measurement errors occur, our objective is to obtain $\hat{\mathbf{q}}^a$ such that its **distance** to \mathbf{q}^a is as small as possible (i.e., we want to minimize the estimation error). We use the l_2 -norm as a measure for the distance between \mathbf{q}^a and $\hat{\mathbf{q}}^a$, defined as:

$$\delta(\mathbf{q}^a, \hat{\mathbf{q}}^a) = \|\mathbf{q}^a - \hat{\mathbf{q}}^a\|_2 = \sqrt{\sum_{i=0}^{n_r-1} (q_i^a - \hat{q}_i^a)^2} \quad (34)$$

The problem of mapping the channel measurements to an estimated channel is non-linear and requires high computations. Two different methods to do this mapping were proposed in [13], namely, i) the ‘‘look-up table’’ method and ii) the ‘‘search’’ method. The look-up table method requires storing a table with entries for all possible channel measurements along with their corresponding channels. This is possible since measurements are quantized using ADCs and hence there exists a finite number of possibilities for \mathbf{y}^s . However, the number of entries in the table could be quite large, especially, if high resolution ADCs are used. On the other hand, the search method requires a combinatorial search over the columns of \mathbf{G} (recall that $\mathbf{y}^s \equiv \mathbf{G}\mathbf{q}^a$) for which the computational complexity is of order $O(n_r^L)$. This could indeed be prohibitive for large antenna arrays. Motivated by the drawbacks of the look-up table and search methods, we propose a new approach that is based on Deep Neural Networks (DNN).

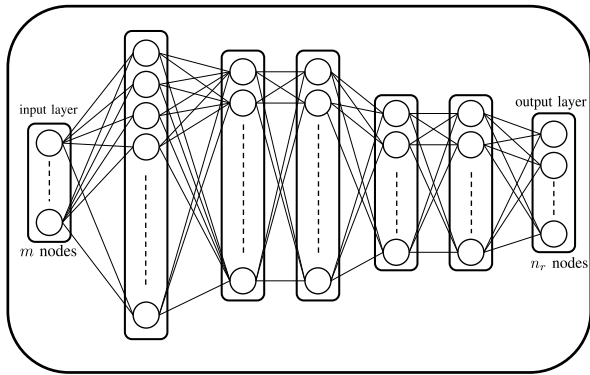


Fig. 4: DNN architecture for mapping measurements of size $m \times 1$ to channels with size $n_r \times 1$. This illustrative model contains 5 hidden layers. Typically, the number of hidden layers and the number of nodes within each layer are design parameters that depend on the channel.

A. DNN-based mapping

Before we delve into describing our proposed model, let us first give a brief introduction to motivate using DNNs. Neural networks (NN) are a class of Machine Learning (ML) algorithms that mimic the human brain. ML is widely used to solve very complex problems through *learning*. We focus on *supervised learning* which is achieved by presenting an algorithm with numerous input examples and their desired outputs. The problem at hand is a multi-dimensional non-linear regression for which neural networks is a powerful tool.

In general, neural networks consist of an input layer, an output layer and one or more hidden layers. Each layer contains several nodes that are interconnected with all nodes of adjacent network layers. Connections between any two nodes carry a certain weight. Adjusting these weights, based on the input-output relationship, is known as *training*. The output of each node is a weighted sum of all input connections passed through an activation function. DNNs are basically neural networks with 2 or more hidden layers. Advantages of DNNs over shallow NNs (with 1 hidden layer) is studied in [23].

DNN model: The DNN model takes the measurement vectors \mathbf{y}^s as an input and produces the corresponding channel estimate $\hat{\mathbf{q}}^a$ at its output. Therefore, the input layer contains m nodes; one for each component in \mathbf{y}^s , while the output layer contains n_r nodes; one for each component of $\hat{\mathbf{q}}^a$. The number of hidden layers and their corresponding number of nodes are design parameters that depend on the sizes of the input and output and the relationship governing them. This architecture is depicted in Fig. 4. For all hidden layers, we use the rectified linear (ReLU) activation function while for the output layer we use the linear activation function. Finally, we use the *ADAM* optimizer [24] (to update the weights) and the Mean Squared Error (MSE) loss function to quantify the model error⁵.

Model training: Although we do not have a closed form expression for mapping \mathbf{y}^s to \mathbf{q}^a (hence the need for an

⁵We use Keras API [25] to build, train, test and use the DNN model we propose. Our pre-trained model and DNN-related codes are available at [?].

algorithmic solution), generating training data is actually straightforward. This is because the reverse direction (i.e., mapping \mathbf{q}^a to \mathbf{y}^s) is just a simple linear transformation. Training data is generated as follows: For every $\mathbf{q}_s^a \in \mathcal{Q}_s^a$ (recall that \mathcal{Q}_s^a is the set of all possible channel support vectors defined in Section IV-B), we generate $n_s = 300$ random channels \mathbf{q}^a by choosing the non-zero components of \mathbf{q}^a to be uniformly distributed in $[-\alpha_{\max}^b, \alpha_{\max}^b]$ where α_{\max}^b is the maximum magnitude of expected baseband path gains which can be obtained using channel statistics (recall Eq. (8)). Thus, the total number of input-output samples we have is $n_s \times |\mathcal{Q}_s^a|$. We use 70% of these samples for training and the remaining 30% for validation. Training is done using 200 epochs with batches of size 32. We monitor the validation error to make sure that the model does not over-fit the training data. If over-fitting is observed (which is indicated by a persistent increase in validation error at the end of every epoch), we stop the training process and only keep the model which produced the least validation error.

B. DNN Model Assessment

To argue the reliability of DNN-based mapping, we will test it using a simple channel with $n_t=1$, $n_r=23$ and a maximum of 3 available channel paths i.e., $L \leq 3$. We also compare the DNN model performance to the “search” method of [13]. Based on the described channel parameters, only $m=11$ measurements are needed for discovering its paths (more details about this particular example are discussed in Section VII). We design a DNN model similar to the one shown in Fig. 4, with an input layer of $m = 11$ nodes and an output layer of $n_r = 23$ nodes. The model also has 5 hidden layers with 1024, 512, 512, 128 and 128 nodes, respectively. We train the DNN model using data generated as described above. Fig. 5a shows the average MSE loss of both training and validation data sets for 100 epochs. The trained model achieves an average validation error of ≈ 0.0143 (averaged across all samples of validation data). The figure also shows close MSE values for training and validation. This indicates that the model generalizes well to measurements it had not seen before which guarantees its reliability for arbitrary future measurements.

These initial results are promising but they are obtained using error-free measurements. Now, we will test the resilience of DNN-based mapping against noisy measurements and compare its performance against the search method proposed in [13]. To do so, we generate a new testing data set, in the same way we created the training data. We also generate sets of uniformly distributed noise vectors where each noise set is drawn at a different value of transmit SNR from -20 to 20 dB. The noise vectors are then added to the inputs (channel measurements) of the testing data set then passed through the trained DNN model. The decoded $\hat{\mathbf{q}}^a$ is recorded at the output. Similarly, we use the “search” method to decode the same noise-corrupted measurements.

For evaluation, we use i) the average MSE, as well as ii) the probability of path misdetection (i.e., no path discovery).

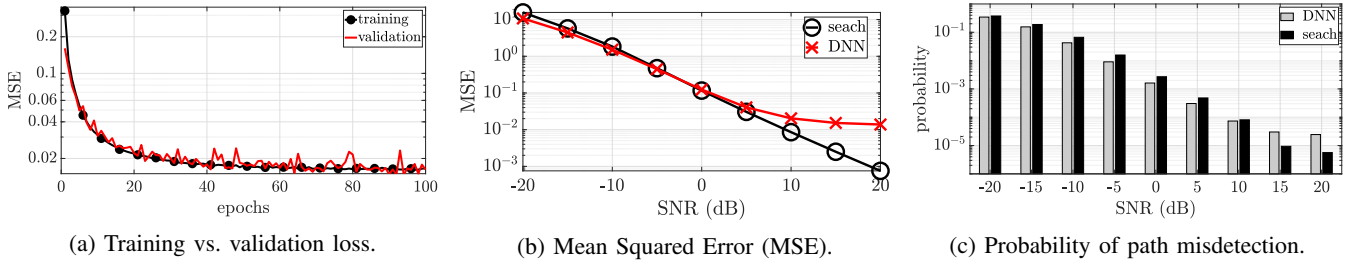


Fig. 5: Evaluation of DNN-based measurement to channel mapping.

We say a path is correctly discovered if the path gain of its corresponding component in \hat{q}^a is among the $L = 3$ strongest components in \hat{q}^a . Fig. 5b shows the average MSE obtained using the search and DNN-based mapping methods on a log scale. We see that at low SNR the DNN-based decoding outperforms the search method. This indicates that the DNN model is more resilient against measurement errors. At high SNR, however, the DNN’s MSE saturates at ≈ 0.014 which is the same value we obtain for validation during model training using noise-free inputs⁶. The search method’s MSE, on the other hand, keeps improving as SNR increases, nevertheless, for values below 10^{-2} , the improvements can be considered marginal. The probability of path misdetection, shown in Fig. 5c, confirms the performance trend of the MSE. Specifically, we see that at low SNR, the DNN-based model outperforms the search method (i.e., has lower probability of misdetection) while at high SNR we see that the search method is better.

Computational complexity: As we have previously discussed, the search method requires high computational power. Precisely, $\binom{23}{3}$ iterations with one matrix inversion and two matrix multiplication operations are performed per iteration, which then produces a vector of length 11. Finally, an additional step of finding the minimum l_2 norm of all $\binom{23}{3}$ vectors is performed. On the other hand, the DNN-based mapping just requires N_k linear computations for the hidden and output layers, where N_k is the number of nodes at the k^{th} layer. These computations are of the form $\sum_{i=1}^{N_{k-1}} w_i a_i$ where a_i is the value passed from the i^{th} node of the previous layer and w_i is the weight on its link. For this particular example, the search method and the DNN-based method were implemented on the same machine and on average the search method’s execution time was 11.2 ms compared to 47 μ s for the DNN model.

VI. MULTIPLE TRANSMIT AND RECEIVE ANTENNAS

Let us do a quick recap of what has been presented so far. Up to this point, we have only dealt with channels with single-transmit, multiple-receive antennas. In Section IV, we explained how to exploit linear source codes in order to obtain channel measurements (encoded channels) with just a few components. We have also shown that there exists a one-to-one mapping between the mm-wave channels and their encoded

counterparts. Then, in Section V, we introduced a method for decoding the measurements using *deep neural networks*.

In this section, we extend the channel setting to be of *multiple-transmit, multiple-receive* antennas. We show how to perform measurements and how to decode them to estimate the whole $n_r \times n_t$ channel. This is essentially achieved by building upon the results of single transmit antenna channels.

A. Measurements

Unlike the single transmit antenna scenario where the TX sends its signals omnidirectionally, it can now focus its transmission on narrow angular directions. However, from the receiver’s point of view, no matter which set of directions the TX is transmitting into, it can only see a number of n_r resolvable bins; only L of which have paths to the TX. The same is true from the transmitter perspective where the TX can only see n_t resolvable bins; only L of which have paths to the receiver⁷. Thus, for an arbitrary tx-precoder, the receiver would need to measure the channel using the same set of w_i ’s it needs for the $n_t = 1$ scenario. The result would be an $n_r \times 1$ angular rx bins corresponding to the particular f_j used at the TX. Similarly, for an arbitrary rx-combiner, the transmitter would need the same set of f_j ’s it would need for the $n_r = 1$ scenario to find its respective tx bins. Thus, to find such f_j ’s and w_i ’s, we can invoke Theorem 3.

Now, let $f_j \forall j \in \{1, \dots, m_t\}$ be the tx-precoding vectors and let $w_i \forall i \in \{1, \dots, m_r\}$ be the rx-combining vectors. Then, the channel measurements are obtained as follows: The transmitter sends a number of m_r pilot symbols using *each* of its m_t precoders. On the receiver side, for every tx-precoder, m_r channel measurements are obtained using the distinct m_r rx-combiners. Recall that

$$u_{i,j} = y_{i,j}^s + w_i^H \mathbf{n} \quad (35)$$

where $y_{i,j}^s = w_i^H \mathbf{Q} \mathbf{f}_j$. Let us arrange the m_r measurements corresponding to the j^{th} tx-precoder in \mathbf{y}_j^s and define \mathbf{Y}^s as

$$\mathbf{Y}^s \triangleq (\mathbf{y}_1^s \quad \mathbf{y}_2^s \quad \dots \quad \mathbf{y}_{m_t}^s) \quad (36)$$

Now \mathbf{Y}^s contains all $m_t \times m_r$ channel measurements necessary to discover all available paths.

⁷Recall that the directions at which the TX is transmitting or the RX is receiving are determined by their antenna beam patterns which are in turn determined by the tx-precoders (f_j) and rx-combiners (w_i), respectively (recall Fig. 2).

⁶The MSE value at which DNN-based mapping saturates can be made lower by further improvement of the DNN model structure shown in Fig. 4.

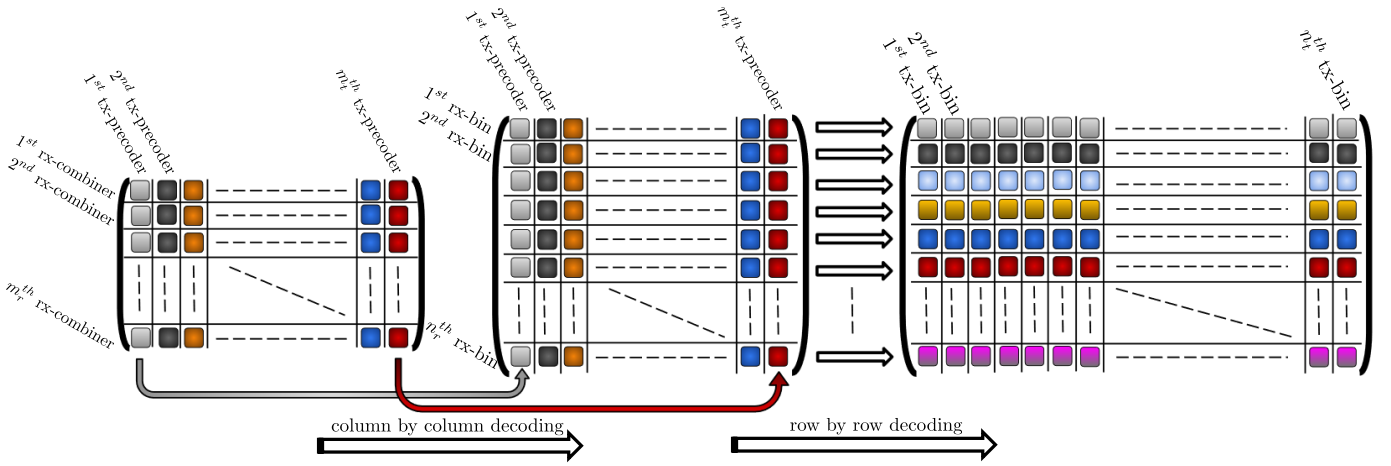


Fig. 6: Measurements decoding for channels with multiple TX/RX antennas is done in two steps. Given the matrix \mathbf{Y}^s whose $y_{i,j}^s$ component is $= \mathbf{w}_i^H \mathbf{Q} \mathbf{f}_j$ (shown on the left), we first do a column by column decoding where the j^{th} decoded column of \mathbf{Y}^s is $\mathbf{q}_{rx,j}^a$. Then, in the second step we decode the intermediary matrix row by row to produce $\hat{\mathbf{Q}}^a$ (shown on the right). The two decoding functions of first and second steps are dependent on the source codes used to design \mathbf{w}_i 's and \mathbf{f}_j 's, respectively.

B. Decoding \mathbf{Y}^s

To obtain $\hat{\mathbf{Q}}^a$ from \mathbf{Y}^s , we will perform multiple SIMO decoding operations as described in Section V. This procedure is highlighted in the diagram shown in Fig. 6 and is detailed as follows:

- (i) Decode every $\mathbf{y}_j^s \forall j \{1, 2, \dots, m_t\}$ to obtain $\mathbf{q}_{rx,j}^a$. Recall that \mathbf{y}_j^s is the measurement vector corresponding to the j^{th} tx-precoder. Thus, $\mathbf{q}_{rx,j}^a$ is the $n_r \times 1$ mm-wave channel observed at RX due to the TX signal transmission through the angular directions defined in \mathbf{f}_j .
- (ii) After step (i) is complete, we obtain a sequence of m_t measurement components corresponding to each rx-bin. Each of these components is produced using a distinct tx-precoder. Let us denote these sequences by $\mathbf{y}_{tx,k}^s$ ($1 \times m_t$ row vectors) where $k \in \{1, 2, \dots, n_r\}$.
- (iii) Decode each $\mathbf{y}_{tx,k}^s$ to obtain $\mathbf{q}_{tx,k}^a$ ($1 \times n_t$ row vectors) whose components constitute all the tx-bins corresponding to the k^{th} rx-bin.
- (iv) Stack all $\mathbf{q}_{tx,k}^a$ vertically to obtain $\hat{\mathbf{Q}}^a$.

VII. PERFORMANCE EVALUATION

In this section, the performance of our proposed source coding-based beam discovery is evaluated. Specifically, simulation⁸ results for mm-wave channels with a maximum number of $L=3$ paths⁹ and $n_t=n_r=23$ antennas are provided. We will consider a variety of finite ADC resolutions as well as the ideal, infinite resolution setting which would help us understand the effect of finite resolution ADCs on performance. We will also provide results for various measurement decoding methods, specifically the DNN-based decoding with and without noise defense as well as the search method

⁸ We used both MATLAB and python to write our simulation codes. We also used tensorflow [26] and Keras [27] for creating, configuring and using DNN models.

⁹Note that L can be obtained from statistical channel models [cite].

proposed in [13]. Now, let us discuss the aspects pertaining to our proposed solution.

A. Performance Metrics

To quantify the performance of our proposed beam discovery solution, we adopt performance metrics that highlight i) the measurement overhead, ii) the accuracy of path discovery and iii) the quality of the estimated path gains. These metrics are evaluated numerically, using Monte Carlo simulations; averaged over 100,000 data points, and evaluated against different values for transmit SNR. We define the performance metrics as follows:

- i) **Number of measurements:** Given by $m_t \times m_r$.
- ii) **Probability of path discovery:** After obtaining a channel estimate $\hat{\mathbf{Q}}^a$, we declare its paths to be existing at the angular directions of its strongest L components.
- iii) **MSE:** Defined as the Frobenius norm $\|\mathbf{Q}^a - \hat{\mathbf{Q}}^a\|_F$.

B. Choice of linear source codes

Recall from our discussion in Section VI-A that we can use Theorem 3 to design both TX and RX measurements (i.e., \mathbf{f}_j 's and \mathbf{w}_i 's). For this example, since $n_r = n_t$, then the same source code will work for designing both tx-precoders and rx-combiners. Thus, we need to find a code whose encoding function \mathcal{E} is injective over the set of support vectors representing all possible tx/rx bins. The **perfect binary Golay code** operating as a syndrome source code is a suitable choice for this problem. This code also achieves the binary entropy if all support vectors of the tx/rx bins have the same probability of occurrence. It has a generator matrix of size 11×22 , hence, we have that $m_t=m_r=11$, and the total number of required channel measurements is $m_t \times m_r=121$. Compared to the exhaustive search approach which requires scanning all combinations of TX/RX angular directions, this represents **75%** reduction in number of measurements.

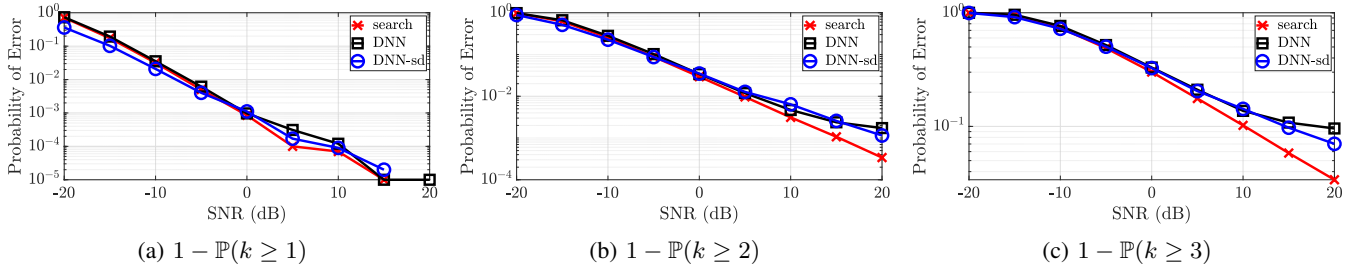


Fig. 7: Beam detection probability for infinite resolution ADCs.

C. DNN model design and training

We design DNNs to have 3 hidden layers, with 6000, 1000 and 250 nodes (neurons) for each layer, respectively. This provides a reasonably good input-to-output mapping performance while keeping the processing speed fairly fast. Two types of DNN training are provided. The first type is error-free training where the training examples are pure, with no added noise components. This is similar to what we did in Section V-B. Measurement errors, however, tend to degrade the performance of path discovery. One way to overcome this impediment is to consider the measurement errors as an “adversarial attack” and to equip the DNN with a defense mechanism against it. The defense we choose for this problem is simply to train the DNN with error-corrupted measurements. This constitutes the second type of training. As will be shown later, this can further enhance the performance of beam discovery.

D. Results

We divide our discussion in this section into two parts. In the first part, we will provide simulation results for infinite resolution ADCs. While impractical, assuming ideal ADCs can help us understand the upper bounds of performance for our proposed beam discovery solution. It also gives an insight into how much resolution is needed to take full advantage of the proposed solution. Results for finite resolution ADCs are provided in the second part of the discussion where the desired ADC resolution is shown to be dependent on the transmit SNR.

1) *Infinite Resolution ADC*: We present the performance of beam discovery using both “search” and “DNN-based” measurement decoding. For the DNN-based method, we present two categories of models; the first category is for models trained using error-free measurements which can be used at all values of transmit SNR, while the second category is for specially trained DNN models with defense against specific noise power values. In other words, the latter category requires a separate DNN model for each level of transmit SNR. We call it “DNN-sd” where “sd” stands for *selective defense*.

Fig. 8 depicts the average MSE of our channel estimates. As shown in the figure, the DNN-based decoding, which is trained using error-free measurements, achieves almost the same performance as the search-based method at almost all SNR values. At very high SNR, however, the search method is better but the improvement is marginal (in the order of 10^{-3}). Interestingly, DNNs that are trained with noisy measurements

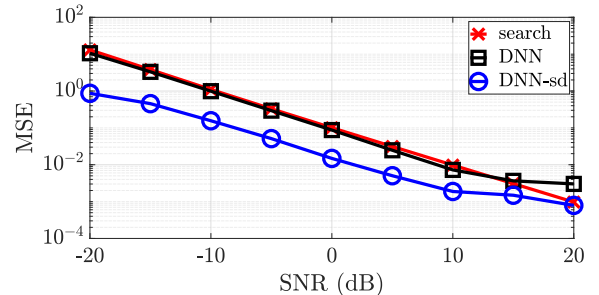


Fig. 8: MSE for infinite resolution ADCs.

(DNN-sd) outperforms both search and DNN. Nevertheless, we can see that at high SNR the DNN-sd’s MSE starts to saturate at $\approx 10^{-3}$ while the search method catches up with it and closes the performance gap.

In Fig 7, we plot the *probability of error* associated with discovering at least k_i channel paths $\forall k_i = \{1, 2, 3\}$ (i.e., $1 - \mathbb{P}(k \geq k_i)$). In other words, we plot the probability of *not* discovering at least k_i paths. This analysis shows that the probability of beam discovery for all three decoding methods are nearly the same except for two key observations: i) At low SNR, Fig. 7a shows a slightly better performance for DNN-sd against both search and DNN. ii) At high SNR, Figs. 7b and 7c show that the search method outperforms both DNN and DNN-sd although its MSE performance was inferior to that of DNN-sd. This could be explained by the fact that all the DNN models we use are trained to minimize the MSE and not directly trained for beam discovery. It also suggests that the channel paths that were not correctly discovered must have a very small gain values which makes them not very useful anyway.

2) *Finite Resolution ADC*: Now, we will shift our focus on finite resolution ADCs. Specifically, we will provide results for ADCs with $b=3, 5$ and 7 bits resolution and compare them against each other and against the ideal ADC case (with $b=\infty$). We will only show the results for “DNN-sd” based decoding since the performance of the other two method follow similar trends to that of the ideal ADCs results shown above.

In Fig. 9, we plot the MSE for various values of b . As expected, we can see that the MSE is inversely proportional to the resolution. We can also see that as SNR increases, more resolution is required to keep the MSE performance close to that of ideal ADCs. For instance, $b=5$ is reasonably good up

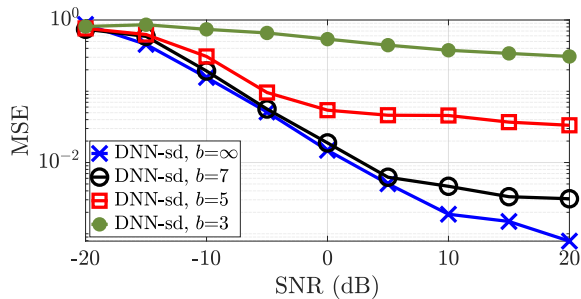


Fig. 9: MSE for various ADC quantization resolutions.

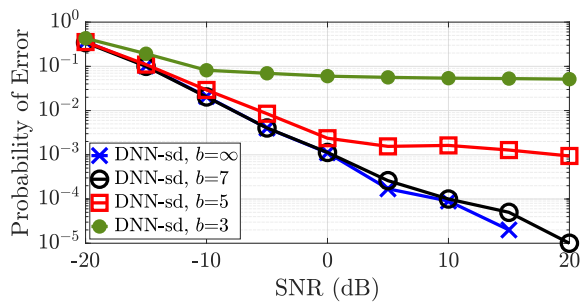


Fig. 10: $1 - \mathbb{P}(k \geq 1)$ for various ADC quantization resolutions.

to $\text{SNR} = -5\text{dB}$. Similarly, the $b=7$ case is very close to $b=\infty$ up to $\text{SNR} = 5\text{dB}$. Even at higher SNR, the $b=7$ has a gap with ideal ADCs that is smaller than $\approx 5 \times 10^{-3}$.

In Fig. 10, we plot the probability of misdetecting all paths and it can be shown that similar trends to the MSE performance can be observed here as well.

VIII. CONCLUSION

This paper tackles the problem of reducing the number of measurements for estimating mmWave channels and treats it as that of source compression. Specifically, we find linear source codes that can uniquely encode all channel matrices, then use them to design the tx-precoders and rx-combiners. The resultant number of measurements depends on the compression ratio of the used codes. Finally, to decode measurements, we use deep neural networks, which provide both high speed and high quality measurement-to-channel mapping.

REFERENCES

- [1] "Cisco visual networking index: Global mobile data traffic forecast update, 2016 - 2021 white paper," Mar 2017. [Online]. Available: <https://goo.gl/U1eQNM>
- [2] T. S. Rappaport, S. Sun, R. Mayzus, H. Zhao, Y. Azar, K. Wang, G. N. Wong, J. K. Schulz, M. Samimi, and F. Gutierrez, "Millimeter wave mobile communications for 5g cellular: It will work!" *IEEE access*, vol. 1, pp. 335–349, 2013.
- [3] Z. Pi and F. Khan, "An introduction to millimeter-wave mobile broadband systems," *IEEE communications magazine*, vol. 49, no. 6, 2011.
- [4] M. R. Akdeniz, Y. Liu, M. K. Samimi, S. Sun, S. Rangan, T. S. Rappaport, and E. Erkip, "Millimeter wave channel modeling and cellular capacity evaluation," *IEEE journal on selected areas in communications*, vol. 32, no. 6, pp. 1164–1179, 2014.
- [5] S. Jog, J. Wang, J. Guan, T. Moon, H. Hassanieh, and R. R. Choudhury, "Many-to-many beam alignment in millimeter wave networks," in *16th {USENIX} Symposium on Networked Systems Design and Implementation ({NSDI} 19)*, 2019, pp. 783–800.
- [6] R. Méndez-Rial, C. Rusu, A. Alkhateeb, N. González-Prelcic, and R. W. Heath, "Channel estimation and hybrid combining for mmwave: Phase shifters or switches?" in *Information Theory and Applications Workshop (ITA)*, 2015. IEEE, 2015, pp. 90–97.
- [7] D. Tse and P. Viswanath, *Fundamentals of wireless communication*. Cambridge university press, 2005.
- [8] S. Rangan, T. S. Rappaport, and E. Erkip, "Millimeter-wave cellular wireless networks: Potentials and challenges," *Proceedings of the IEEE*, vol. 102, no. 3, pp. 366–385, 2014.
- [9] J. W. Choi, B. Shim, Y. Ding, B. Rao, and D. I. Kim, "Compressed sensing for wireless communications : Useful tips and tricks," *IEEE Communications Surveys Tutorials*, vol. PP, no. 99, pp. 1–1, 2017.
- [10] H. Hassanieh, O. Abari, M. Rodriguez, M. Abdelghany, D. Katabi, and P. Indyk, "Fast millimeter wave beam alignment," in *Proceedings of the 2018 Conference of the ACM Special Interest Group on Data Communication*. ACM, 2018, pp. 432–445.
- [11] Y. Shabara, C. E. Koksall, and E. Ekici, "Linear block coding for efficient beam discovery in millimeter wave communication networks," in *IEEE INFOCOM 2018-IEEE Conference on Computer Communications*. IEEE, 2018, pp. 2285–2293.
- [12] T. Ancheta, "Syndrome-source-coding and its universal generalization," *IEEE Transactions on Information Theory*, vol. 22, no. 4, pp. 432–436, Jul 1976.
- [13] Y. Shabara, C. E. Koksall, and E. Ekici, "Linear block coding for efficient beam discovery in millimeter wave communication networks," *arXiv preprint arXiv:1712.07161*, 2017.
- [14] C.-K. Wen, C.-J. Wang, S. Jin, K.-K. Wong, and P. Ting, "Bayes-optimal joint channel-and-data estimation for massive mimo with low-precision adcs," *IEEE Transactions on Signal Processing*, vol. 64, no. 10, pp. 2541–2556, 2016.
- [15] J. Mo, P. Schniter, and R. W. Heath, "Channel estimation in broadband millimeter wave mimo systems with few-bit adcs," *IEEE Transactions on Signal Processing*, vol. 66, no. 5, pp. 1141–1154, 2018.
- [16] T. Wang, C.-K. Wen, H. Wang, F. Gao, T. Jiang, and S. Jin, "Deep learning for wireless physical layer: Opportunities and challenges," *China Communications*, vol. 14, no. 11, pp. 92–111, 2017.
- [17] H. He, C.-K. Wen, S. Jin, and G. Y. Li, "Deep learning-based channel estimation for beamspace mmwave massive mimo systems," *IEEE Wireless Communications Letters*, vol. 7, no. 5, pp. 852–855, 2018.
- [18] H. Huang, J. Yang, H. Huang, Y. Song, and G. Gui, "Deep learning for super-resolution channel estimation and doa estimation based massive mimo system," *IEEE Transactions on Vehicular Technology*, vol. 67, no. 9, pp. 8549–8560, 2018.
- [19] A. Alkhateeb, O. El Ayach, G. Leus, and R. W. Heath, "Channel estimation and hybrid precoding for millimeter wave cellular systems," *IEEE Journal of Selected Topics in Signal Processing*, vol. 8, no. 5, pp. 831–846, 2014.
- [20] J. Mo, P. Schniter, N. G. Prelcic, and R. W. Heath, "Channel estimation in millimeter wave mimo systems with one-bit quantization," in *2014 48th Asilomar Conference on Signals, Systems and Computers*, Nov 2014, pp. 957–961.
- [21] M. Kokshoorn, H. Chen, P. Wang, Y. Li, and B. Vucetic, "Millimeter wave mimo channel estimation using overlapped beam patterns and rate adaptation," *IEEE Transactions on Signal Processing*, vol. 65, no. 3, pp. 601–616, Feb 2017.
- [22] D. Grinberg, "Notes on the combinatorial fundamentals of algebra," 2016.
- [23] S. Liang and R. Srikant, "Why deep neural networks," *CoRR*, 2016.
- [24] D. P. Kingma and J. Ba, "Adam: A method for stochastic optimization," *arXiv preprint arXiv:1412.6980*, 2014.
- [25] F. Chollet *et al.*, "Keras," <https://keras.io>, 2015.
- [26] M. Abadi, P. Barham, J. Chen, Z. Chen, Davis *et al.*, "Tensorflow: A system for large-scale machine learning," in *12th {USENIX} Symposium on Operating Systems Design and Implementation ({OSDI} 16)*, 2016, pp. 265–283.
- [27] F. Chollet *et al.*, "Keras," 2015.